Promotion of an Antitumor Immune Program by a Tumor-specific, Complement-activating Antibody

Ruchi Saxena,* Ryan T. Bushey,† Michael J. Campa,† Elizabeth B. Gottlin,† Jian Guo,* Edward F. Patz, Jr,†,‡ and You-Wen He*

Tumor-targeting Abs can be used to initiate an antitumor immune program, which appears essential to achieve a long-term durable clinical response to cancer. We previously identified an anti–complement factor H (CFH) autoantibody associated with patients with early-stage non–small cell lung cancer. We cloned from their peripheral B cells an mAb, GT103, that specifically recognizes CFH on tumor cells. Although the underlying mechanisms are not well defined, GT103 targets a conformationally distinct CFH epitope that is created when CFH is associated with tumor cells, kills tumor cells in vitro, and has potent antitumor activity in vivo. In the effort to better understand how an Ab targeting a tumor epitope can promote an effective antitumor immune response, we used the syngeneic CMT167 lung tumor C57BL/6 mouse model, and we found that murinized GT103 (mGT103) activates complement and enhances antitumor immunity through multiple pathways. It creates a favorable tumor microenvironment by decreasing immunosuppressive regulatory T cells and myeloid-derived suppressor cells, enhances Ag-specific effector T cells, and has an additive antitumor effect with anti-PD-L1 mAb. Furthermore, the immune landscape of tumors from early-stage patients expressing the anti-CFH autoantibody is associated with an immunologically active tumor microenvironment. More broadly, our results using an mAb cloned from autoantibody-expressing B cells provides novel, to our knowledge, mechanistic insights into how a tumor-specific, complement-activating Ab can generate an immune program to kill tumor cells and inhibit tumor growth. ***The Journal of Immunology*****, 2024, 212: 1589–1601.**

The use of mAbs has become a major modality for cancer treatment; however, their full potential has yet to be realized. Abs have been shown to initiate allogeneic tumor rejection (1) that ultimately results in adaptive immunity and tumor regression (2). Any tumor-targeting Ab that not only could kill tumor cells directly but also would stimulate antitumor immunity would undoubtedly promote a more durable clinical response.

Given the specificity and therapeutic potential of mAbs, we previously sought to determine if there were autoantibodies from patients with cancer that could be developed as a novel therapy. We reported that patients with early-stage non–small cell lung cancer (NSCLC) with exceptional outcomes who never develop metastasis or recurrence after surgical resection showed higher incidences of autoantibodies to complement factor H (CFH) than patients with NSCLC with late-stage disease (3, 4). We further characterized these autoantibodies and found that they recognize a conformationally distinct epitope of CFH hypothesized to be presented on tumor cells but not exposed on normal cells (4). The Abs increased C3b deposition and caused complement-dependent lysis of tumor cells (4). We cloned 15 fully human anti-CFH mAbs from individual peripheral B cells of patients with NSCLC (5). The lead therapeutic candidate, mAb7968/GT103, recognizes a tumor-specific, conformationally distinct epitope of CFH located in short consensus repeat (SCR) domain 19 as confirmed by X-ray crystallography (6). Although CFH inhibits the alternative pathway of complement activation, GT103 does not directly affect this pathway; rather, GT103 kills tumor cells in vitro by activating the classical complement pathway and causes Ab-dependent cellular phagocytosis (6, 7). GT103 inhibits tumor growth in both patient-derived brain tumor xenograft-bearing nude mice and wild-type (WT) syngeneic lung cancer models with no effect on normal tissues (5, 6). It has been reported that autoantibodies against the CFH SCR 19–20 domains are associated with atypical hemolytic uremic syndrome (8). However, we showed that GT103 binds to CFH on tumor tissues but not to normal lung and kidney from mouse and human (7). The kidneys in GT103-treated tumor-bearing mice showed no signs of damage or toxicity,

*Department of Integrative Immunobiology, Duke University School of Medicine, Durham, NC; †Department of Radiology, Duke University School of Medicine, Durham, NC; and ‡Department of Pharmacology and Cancer Biology, Duke University School of Medicine, Durham, NC

ORCIDs: 0000-0002-9945-5384 (R.S.); 0000-0003-2497-4953 (R.T.B.); 0000-0003-4146-2706 (M.J.C.); 0000-0003-0886-0024 (E.B.G.); 0000-0003-3374-1596 (E.F.P.); 0000-0002-8983-2684 (Y.-W. H.).

Received for publication November 1, 2023. Accepted for publication March 4, 2024.

This work was supported by the U.S. Department of Defense through Lung Cancer Research Program Translational Research Partnership Award No. W81XWH-19-1-0342 (to E.F.P. and Y.-W.H.) and by an award from the Sunny Li Family Fund (to Y.-W.H.).

R.S., R.T.B., M.J.C., and J.G. performed experiments. R.S., E.F.P., and Y.-W.H. designed the project. R.S., R.T.B., M.J.C., E.B.G., E.F.P., and Y.-W.H. analyzed the data. R.S. and Y.-W.H. wrote the paper. All authors read, edited, and approved the manuscript.

The raw sequence data reported in this paper have been deposited in the Sequence Read Archive in the National Library of Medicine, National Center for Biotechnology Information (https://www.ncbi.nlm.nih.gov). The raw data for bulk RNA-sequencing analysis are available under Bioproject accession number PRJNA936632. All the other data supporting the findings of this study are available within the article and its supplemental information files and from the corresponding author upon reasonable request. Source data are provided with this paper. GT103 mAb is available upon appropriate material transfer agreement.

Address correspondence and reprint requests to Prof. You-Wen He and Prof. Edward F. Patz, Jr., Box 3010, Duke University Medical Center, Durham, NC 27710 (Y.-W.H.); and Box 3808, Duke University Medical Center, Durham, NC 27710 (E.F.P.). E-mail addresses: youwen.he@duke.edu (Y.-W.H.) and patz0002@mc.duke.edu (E.F.P.)

The online version of this article contains supplemental material.

Abbreviations used in this article: aTreg, adipose regulatory T cell; CDC, complement dependent cytotoxicity; CFH, complement factor H; CR2, complement receptor 2; CR3, complement receptor 3; CVF, cobra venom factor; DAMP, damage-associated molecular pattern; DC, dendritic cell; FDR, false discovery rate; FSC, forward scatter; HMGB1, high mobility group box 1 protein; IMC, imaging mass cytometry; itTreg, intratumoral regulatory T cell; KO, knockout; MDSC, myeloid-derived suppressor cell; NSCLC, non–small cell lung cancer; poly(I:C), polyinosinic-polycytidylic acid sodium salt; RNA-seq, RNA sequencing; ROS, reactive oxygen species; SCR, short consensus repeat; scRNAseq, single-cell RNA sequencing; TAN, tumor-associated neutrophil; TIL, tumor-infiltrating lymphocyte; TME, tumor microenvironment; Treg, regulatory T cell; WT, wild type.

https://doi.org/10.4049/jimmunol.2300728

suggesting that GT103 treatment does not cause adverse effects in kidneys.

The complement system has an intricate relationship with cancer. Activation of the complement cascade may generate anti- or protumor effects in a highly context-dependent manner (9, 10). CFH is an abundant serum protein whose primary function is to regulate complement activation and protect host cells, including tumor cells, from attack and destruction by the alternative pathway of complement-mediated cytotoxicity (11). Although CFH is primarily produced by the liver, many different tumor cell types express CFH (12–19). Furthermore, higher expression of CFH in lung adenocarcinoma correlates with worse outcome (20, 21). CFH may exert several suppressive effects on host antitumor immunity. First, it protects tumor cells from complement-mediated killing (12–15, 17–19). Second, CFH produced by tumor cells promotes $CD14^+$ monocyte differentiation into immune-suppressive ($HLA\text{-}DR^{low}PD\text{-}L1^{hi}$) macrophages (16). Third, CFH promotes differentiation of tolerogenic and anti-inflammatory monocyte-derived dendritic cells (DCs). CFH-treated monocyte-derived DCs resembled immature DCs, inhibited allostimulated T cell activation, and induced regulatory T cell (Treg) production (22). Fourth, CFH expressed on tumor extracellular vesicles promotes tumorigenesis and metastasis by inhibiting complement-mediated cell killing (23).

Although we have established that GT103 has antitumor activities in tumor models, the underlying immune program generated by GT103 remains poorly characterized. In this study, we investigated GT103-mediated antitumor effects at the cellular and molecular levels and demonstrated that GT103 enhances antitumor immunity through multiple pathways. GT103 treatment causes complement activation in vivo and creates a favorable tumor microenvironment (TME) by decreasing immunosuppressive Tregs and myeloid-derived suppressor cells (MDSCs) and enhancing Ag-specific effector T cells. Our results provide mechanistic insights into this novel, to our knowledge, immunotherapeutic agent and underscore the potential of a functional autoantibody in promoting an effective antitumor immune program.

Materials and Methods

Cell lines and reagents

The mouse CMT167 lung tumor cell line was a kind gift from Raphael Nemenoff (University of Colorado). CMT167 was tested for mycoplasma and found to be negative before use in animal experiments. The CMT167 cell line expressing membrane-bound chicken OVA (CMT167-OVA) was produced using an expression plasmid (pcDNA3-OVA) containing cDNA encoding full-length OVA protein linked to the transmembrane region of H-2Kb. B16F10 melanoma cells stably expressing chicken OVA (B16F10-OVA) were provided by Dr. Thomas F. Tedder (Duke University). The cell lines were maintained in RPMI 1640 medium (Life Technologies) containing 10% FBS (USA Scientific), 2 mM glutamine, and 50 μg/ml gentamicin at 37°C and 5% CO_2. For the mouse studies, a murine version of GT103 (mGT103) was used that has been characterized previously (5). mGT103 retains the same CDRs as the human Ab placed in an IgG2a murine backbone. The epitope in mouse and human CFH is identical, and mGT103 and human GT103 recognize a peptide containing the epitope with similar affinities (5).

Mice and tumor models

All studies were approved by the institutional animal care and use committee at Duke University. The in vivo studies were performed in WT syngeneic mice with an intact complement system, and thus the effect of GT103 observed was in the presence of physiological levels of complement. All experiments were randomized and blinded when possible. Six- to 8-wk-old C57BL/6 mice were implanted s.c. in the right flank with either 2.0×10^5 CMT167 cells, B16F10-OVA, CMT167-OVA cells, or CFH-knockout (CFH-KO) CMT167 cells.

One week after inoculation, mice were randomly grouped with 6–10 mice per group and treated for 2 wk with i.p. injections of a control solution (murine IgG2 or PBS) or mGT103 (200 μg/mouse) thrice weekly. Bidimensional tumor measurements were made every other day, and tumor volume was calculated using the equation $V = (\text{smaller diameter})^2 \times (\text{larger diameter}/2)$. After the mice were sacrificed, tumors were excised and weighed, and a portion of the tissue was stored in RNA*later* for RNA studies. A portion of the excised tumors was used to prepare single-cell suspensions of tumor-infiltrating lymphocytes (TILs) for flow cytometry.

To deplete complement factor C3, CMT167 cells were inoculated, and, after the tumors became palpable, mice were injected i.p. with 10 μg/mouse of cobra venom factor (CVF) (Calbiochem; catalog no. 233552) 4 h before being injected with IgG2 or mGT103. Thereafter, mice were treated with IgG2 control Ab (200 μg/mouse i.p. thrice weekly), mGT103 (200 μg/mouse i.p. thrice weekly), and CVF (10 μg/mouse twice weekly) for 24 d. Tumors were measured every other day, and, at the end of the treatment period, mice were sacrificed and their tissues were collected. For C3aR and C5aR blockade, mice were injected i.p. with a 1 mg/kg dose of C3aR antagonist, SB 290157 (Calbiochem; catalog no. SB290157) (24), and C5aR antagonist, PMX53 (Calbiochem; catalog no. 533683) (25), 2 h before IgG2 or mGT103 and thereafter twice weekly for 24 d.

For comparison between GT103 and other known immunotherapeutic agents and to find a combination with better therapeutic efficacy, mice were treated with anti-OX40 Ab (Bio X Cell) (200 μg/mouse i.p. thrice weekly), anti-CTLA4 Ab (Bio X Cell) (200 μg/mouse i.p. thrice weekly), anti-CD47 Ab (Bio X Cell) (200 μg/mouse i.p. thrice weekly), CD40 agonist Ab (Bio X Cell) (200 μg/mouse i.p. thrice weekly), or anti-PD-L1 (Bio X Cell) (200 μg/mouse i.p. thrice weekly) Ab either alone or in combination with mGT103 for the length of the experiment. For combination therapy, we also treated the mice with a combination of mGT103 and polyinosinic-polycytidylic acid sodium salt [poly(I:C)] (20 μg/mouse i.p. thrice weekly) or with a combination of mGT103, anti-PD-L1 and poly(I:C). Tumors were measured as before, and, at the end of the treatment period, mice were sacrificed and their tumor tissue was saved for further processing. For CD4 and CD8 T cell depletion in vivo, mice were administered anti-CD4 and anti-CD8 Abs (BioLegend, San Diego, CA) (100 μg/mouse i.p.) on the day of tumor inoculation and once every week thereafter. Details of the therapeutic and depleting Abs used are provided in Supplemental Table S1.

Preparation of single-cell suspensions and flow cytometry

Single-cell suspensions from tumor tissue and lymph nodes were prepared and analyzed for different immune cell populations by flow cytometry. Briefly, the tissues were minced using scissors and incubated with 200 U/ml collagenase (Thermo Fisher Scientific, Waltham, MA) and 100 U/ml DNase I (Sigma-Aldrich, St. Louis, MO) in RPMI for 30 min at 37°C. Single-cell suspensions were stained with fluorescently conjugated Abs (BioLegend) against CD45, CD19, CD3, CD4, CD8a, perforin, Gr-1, CD11b, FoxP3, CD11c, CD14, and NK1. Details of the Abs are provided in Supplemental Table S1. Intracellular staining for FOXP3 and perforin was carried out using BD Cytofix/Cytoperm Fixation/Permeabilization Solution Kit as per the manufacturer's instructions. Ag-specific CD4+ and CD8+ tumor-infiltrating cells were analyzed using allophycocyanin-conjugated I-Ab/OVA 323–339 MHC II (catalog no. TS-M710-2) and PE-conjugated H-2Kb/OVA 257–264 MHC I (catalog no. TB-5001-1) peptide tetramer probes, respectively, from MBL International Corporation, Woburn, MA. Tetramer staining was carried out in accordance with the manufacturer's suggested protocol. Flow cytometric analysis was performed on a FACSCanto flow cytometer (BD Biosciences), and the results were analyzed using FlowJo software.

The gating strategy included selection of intact and single cells by gating in a forward scatter (FSC) versus side scatter plot to exclude debris and cell aggregates. Single cells were then selected by plotting FSC-A versus FSC-H. Live/Dead stain (Thermo Fisher Scientific; catalog no. L34955) was used to exclude dead cells, and then $CD45^+$ cells were selected for further characterization and subpopulation analysis based on specific markers.

Immunofluorescence imaging

Frozen tumors were cut into 7-μm sections and placed on slides. Samples were fixed in 4% paraformaldehyde for 15 min and permeabilized with 0.25% Triton X-100 in PBS for 10 min at room temperature. Blocking was performed with 5% goat serum in PBS-T (PBS with 0.1% Tween 20) for 1 h at room temperature. Slides were incubated with anti-HMGB1 Ab (Abcam; catalog no. Ab79823) diluted 1:250 in 1% BSA in PBS overnight at 4°C and an Alexa Fluor 488 goat anti-rabbit secondary Ab (Invitrogen; catalog no. A11008) at 10 μg/ml in 1% BSA in PBS for 2 h at room temperature. Slides were washed four times in PBST following primary and secondary Ab incubations. Slides were incubated with Hoechst 33342 DNA stain (Thermo Fisher Scientific; catalog no. 62249) at 1 μg/ml for 5 min at room temperature, and Prolong Gold (Thermo Fisher Scientific; catalog no. P10144) was

used as the mountant. Microscopy was performed at original magnification ×40 using the Zeiss Axio Imager widefield fluorescence microscope.

Western blot analysis

Whole-cell lysate from tumor tissues from IgG2- and GT103-treated mice were prepared using radioimmunoprecipitation assay buffer supplemented with protease inhibitor mixture (Abcam) and PMSF (100 μg/ml; Sigma-Aldrich). Lysates were fractionated in 8–16% gradient SDS-polyacrylamide gels, and the separated proteins were transferred to PVDF membranes. The blots were blocked using 5% nonfat dry milk and then probed with anti-C3d (R&D Systems; AF2655) or anti-HMGB1 (Abcam; Ab79823) Ab followed by a secondary rabbit anti-goat HRP Ab (Santa Cruz Biotechnology; sc2768) or goat anti-rabbit HRP Ab (Santa Cruz Biotechnology; sc2054) and then incubated with SuperSignal chemiluminescence substrate (Pierce, Rockford, IL). Membranes were stripped and reprobed with anti-β-actin Ab (R&D Systems; MAB8929) as a loading control. Blots were analyzed by densitometry using the Bio-Rad Laboratories ChemiDoc imaging system, and quantitation was done using ImageJ software. The experiment was performed in triplicate.

RNA sequencing

Total RNA was isolated from tumor tissue using Purelink RNA Minikits (Ambion, Life Technologies) according to the manufacturer's instructions. The KAPA Stranded mRNA-seq library prep kit was used to make sequencing libraries, and libraries were sequenced on Illumina instruments with a 50-bp single-end read length.

RNA-sequencing (RNA-seq) data were processed using the TrimGalore toolkit, which employs Cutadapt to trim low-quality bases and Illumina sequencing adapters from the 3′ end of the reads. Only reads that were 20 nucleotides or longer after trimming were kept for further analysis. Reads were mapped to the GRCm38v73 version of the mouse genome and transcriptome using the STAR RNA-seq alignment tool. Reads were kept for subsequent analysis if they mapped to a single genomic location. Gene counts were compiled using the HTSeq tool. Only genes that had at least 10 reads in any given library were used in subsequent analysis. Normalization and differential expression detection were carried out using the DESeq2 Bioconductor package with the R statistical programming environment. The false discovery rate (FDR) was calculated to control for multiple hypothesis testing. Gene set enrichment analysis was performed to identify gene ontology terms and pathways associated with altered gene expression for each of the comparisons performed.

Cytokine array analysis

Blood was collected from the submandibular vein of IgG2 control– and mGT103-treated mice at day 0, before treatment, and at day 15, after treatment. Serum samples were prepared and then applied to the RayBiotech C1000 Ab array as per the manufacturer's protocol. Membranes were analyzed by densitometry using the Bio-Rad Laboratories ChemiDoc imaging system, and quantitation was done using ImageJ software. The experiment was performed in triplicate.

Single-cell RNA sequencing

Single-cell suspensions of TILs from pooled tumor tissue from three mice in each group were prepared, and $CD45^+$ cells were sorted by FACS. Briefly, the tissues were minced using scissors and incubated with 200 U/ml collagenase and 100 U/ml DNase I in RPMI for 30 min at 37°C. The cell suspensions were filtered through a 40-μm cell strainer, washed twice with PBS, and stained with anti-allophycocyanin/cyanine 7-CD45 Ab (catalog no. 130116; BioLegend) in PBS containing 2% FBS for 30 min at 4°C. To exclude dead cells, the cells were stained with Live/Dead Fixable Aqua dead stain (Invitrogen; catalog no. L34957). Cells were then washed with staining buffer and suspended in RPMI containing 5% FBS. $CD45^+$ cells were sorted using an Asterios cell sorter (BD Biosciences) into Dulbecco's PBS + 0.04% BSA at a concentration of 1×10^6 cells/ml and retained on ice. Sorted cells were then counted and assessed for viability with Trypan blue using a Countess II automated counter (Thermo Fisher Scientific). The cells were then resuspended at $1–2 \times 10^5$ cells/ml with a final viability of >90%. Single cells were encapsulated into emulsion droplets using a Chromium Controller (10X Genomics). Single-cell RNA-sequencing (scRNAseq) libraries were constructed using Chromium Single Cell 3′ Reagent Kits version 3 (10X Genomics) according to the manufacturer's protocol. Reverse transcription and library preparation were performed on a Veriti Thermal Cycler with 96-Deep Well Reaction Module (Thermo Fisher Scientific). Amplified cDNA was purified using SPRIselect beads (Beckman Coulter) and sheared to 250–400 bp. Qualification was performed using a Qubit 3.0 fluorometer. Sequences were subjected to standard quality control, filtering, normalization, sample integration, and clustering steps, and analysis of differential gene expression between the two groups was performed as described using the Seurat R package as described (26–28). R package Single Rv1.4.0 (29) was used to annotate cell types on the basis of correlation profiles with the murine ImmGen (30) reference data set. Differential expression analyses were performed using the function *FindMarkers* implemented in the Seurat package with a Wilcoxon rank-sum test (test.use = 'wilcox'). To test all genes expressed in the data set, the following arguments were changed from default: logfc. threshold = -Inf, min.pct = -Inf, min. cells. group = -Inf.

Imaging mass cytometry

To investigate the TME of NSCLC, we selected a set of 10 adenocarcinoma stage I tumors, which consisted of five from CFH autoantibody-positive patients and five from CFH autoantibody-negative patients. The human samples used in this study were collected between 1998 and 2022 under an institutional review board–approved biomarker protocol (Pro00012914), and all patients signed informed consent forms. The protocol attempted to recruit all patients, regardless of age, sex, and race identified from Duke University Medical Center clinics with a new diagnosis of primary lung cancer. All patients enrolled for this study had blood and tissue collected at the time of initial diagnosis.

A panel of 22 imaging mass cytometry (IMC) metal-conjugated Abs was designed for human lung cancer analysis. This panel included markers for tumor cells, vascular epithelial cells, and immune cells (Supplemental Table S1). Preconjugated metal-labeled Abs, purchased from Fluidigm, were tested for specificity according to the company datasheet. A human lung tumor tissue microarray containing the 10 lung adenocarcinoma specimens was sectioned into 5-μm sections, which were placed on silane-coated glass sides and stained using standard immunohistochemical methods. Briefly, slides were incubated for 1 h at 60°C on a slide warmer followed by dewaxing in xylene and sequential rehydration steps followed by Ag retrieval in 10 mM citrate buffer, pH 6. To decrease nonspecific Ab binding, the microarray was blocked with 3% BSA and incubated overnight at 4°C with the panel of metal-conjugated primary Abs in 0.5% BSA with 0.1% Triton X-100. The next day, slides were washed twice in 0.2% Triton X-100 in PBS and twice in TBS. DNA staining was performed using Intercalator-Iridium in PBS solution for 30 min in a humid chamber at room temperature. Slides were washed with Milli-Q water and air dried before ablation. The slides were imaged with a Hyperion Imaging System in the Cell Analysis and Cytometry Core at the Petit Institute for Bioengineering and Bioscience at the Georgia Institute of Technology. Ab staining of tissue sections was quantified through laser ablation using a modified ArF excimer GeoLas C laser system (Coherent) in a rastered pattern at 20 Hz and direct aerosol transportation of the sample to a cytometry by time of flight mass cytometer (Fluidigm). Cell segmentation was performed using MCDViewer and CellProfiler 4.2.1. MCDViewer was used to classify pixels into three classes (nuclei, membrane, and background) and to generate probability maps. CellProfiler was used to segment probability maps to generate segmentation masks. A combination of channels was used to classify the background and membrane. These masks were combined with the individual .tiff files to extract single-cell information from each individual image. Further image analysis was performed using HistoCAT_1.73 software (31).

Statistical analysis

GraphPad Prism was used for statistical analysis, and the differences between groups were calculated using one-way ANOVA and Student *t* test. A p value <0.05 was considered statistically significant. The numbers of biological replicates were determined on the basis of published studies and pilot experiments and were sufficient to produce statistically significant differences.

Results

GT103 creates a favorable antitumor microenvironment

To investigate the cellular mechanisms of GT103, we treated mice bearing s.c. CMT167 lung tumors with a murinized version of GT103 (mGT103) having the same CDRs as human GT103 or with PBS. mGT103 treatment resulted in significant tumor growth inhibition (Fig. 1A). We also tested the antitumor effect of mGT103 in a B16F10-OVA melanoma tumor model and found similar antitumor efficacy (Fig. 1B). Thus, together with our published data (5), mGT103 has antitumor activities across different tumor models. To determine the cellular mechanisms underlying the antitumor effect of GT103, we analyzed tumor-infiltrating leukocytes from CMT167 tumors. The percentages of intratumoral Tregs and MDSCs

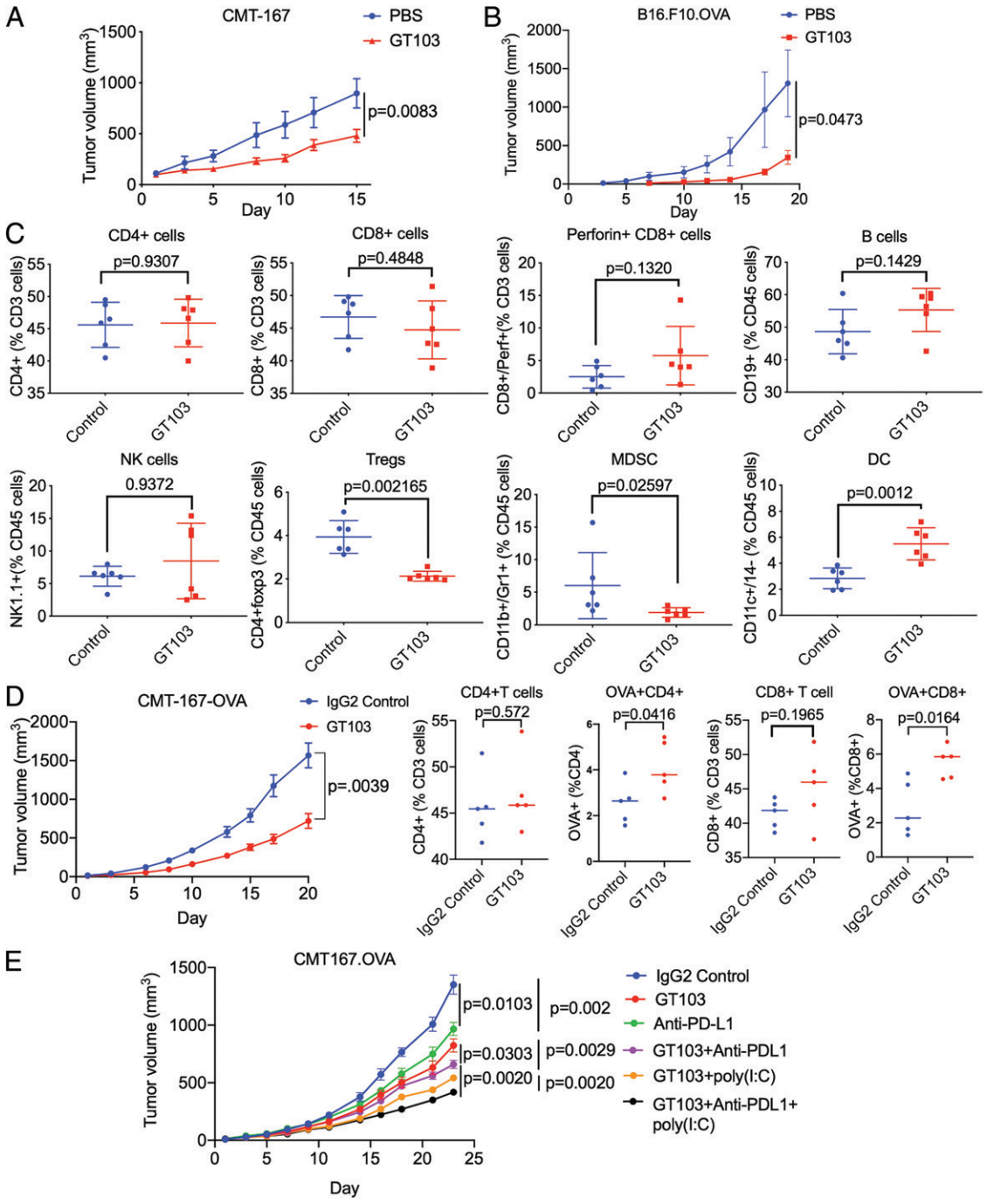

FIGURE 1. Effect of GT103 on tumor growth and tumor-infiltrating leukocytes. Growth of (**A**) syngeneic CMT167 tumors and (**B**) B16F10-OVA tumors in C57BL/6 mice after PBS and mGT103 treatment. Tumor volume was plotted as mean ± SEM (n = 10) for each treatment group. (**C**) Percentage of tumor-infiltrating leukocytes isolated from the CMT167 dissected tumors as analyzed by flow cytometry. (**D**) Growth of syngeneic CMT167-OVA tumors after IgG2a isotype control Ab and mGT103 treatment. Tumor volume was plotted as mean ± SEM (n = 10) for each treatment group. Percentage of total tumor-infiltrating $CD4^+$, $CD8^+$ T cells and OVA-specific cells isolated from the CMT167 dissected tumors as analyzed by flow cytometry. (**E**) Antitumor efficacy of combining mGT103 with anti-PD-L1 Ab and adjuvant poly(I:C). Growth of syngeneic CMT167-OVA tumors in C57BL/6 mice after treatment with IgG2a, mGT103, or anti-PD-L1 Ab as monotherapy or with combinations of GT103 with anti-PD-L1 and/or poly(I:C). Tumor volume was plotted as mean ± SEM (n = 5–7) for each treatment group.

were significantly lower, whereas intratumoral $CD11c^+$ DCs were significantly higher, in the tumors of mGT103-treated mice than those in control tumors (Fig. 1C). The percentages of intratumoral total B lymphocytes and the $perforin^+$ effector $CD8^+$ subset exhibited an increasing trend in mGT103-treated tumors that did not reach statistical significance (Fig. 1C). The total $CD4^+$ and $CD8^+$ TILs were not significantly different between mGT103- and control-treated groups (Fig. 1C).

We further analyzed tumor-specific effector $CD4^+$ and $CD8^+$ T cells using CMT167 lung cancer cells stably expressing chicken OVA (CMT167-OVA). mGT103 treatment significantly inhibited growth of CMT167-OVA tumors when compared with the murine IgG2-treated control group (Fig. 1D). OVA peptide-specific $CD4^+$ and $CD8^+$ TIL frequencies were analyzed using allophycocyanin-conjugated I-Ab/OVA 323–339 MHC II and PE-conjugated H-2Kb/OVA 257–264 MHC I peptide tetramer probes, respectively.

Intratumoral Ag-specific $CD4^+$ and $CD8^+$ cells were significantly increased upon mGT103 treatment (Fig. 1D).

Taken together, these data demonstrate that mGT103 has antitumor efficacy in lung cancer and melanoma models and promotes a favorable antitumor microenvironment with decreased Tregs and MDSCs, increased DCs, and enhanced Ag-specific $CD4^+$ and $CD8^+$ T cells.

Antitumor efficacy of combination immunotherapy of GT103 with PD-L1 blockade and adjuvant poly(I:C)

Given the prominent role of immune checkpoint inhibitors in cancer immunotherapy and our data that showed GT103 reduces the local tumor immunosuppressive environment and promotes an adaptive response, we tested mGT103 in combination with other immunotherapeutic agents. Although mGT103, anti-OX40, anti-CD47, and CD40 agonist Abs as single agents reduced the growth of CMT167-OVA tumors, anti-CTLA4 Ab alone did not limit the growth of these tumors. The combination of mGT103 with anti-OX40, anti-CTLA4, and CD40 agonist Abs did not provide any additive therapeutic effect over the monotherapies. We observed that combination of mGT103 with anti-CD47 Ab exhibited better antitumor efficacy than either agent alone, but it did not reach statistical significance (Supplemental Fig. 1).

Next, we compared the antitumor effect of mGT103 with that of anti-PD-L1 monotherapy and in combination therapy with mGT103. mGT103 and anti-PD-L1 had comparable antitumor efficacy when used as monotherapy (Fig. 1E). When the two agents were used in combination, an increased effect was observed (Fig. 1E). We further tested the effect of combining mGT103 with an adjuvant, poly(I:C), a TLR3 agonist. Interestingly, the combination worked better to reduce tumor growth in mice than mGT103, anti-PD-L1 monotherapy, or the combination of mGT103 and anti-PD-L1. A further decrease in tumor growth was observed when the three agents mGT103, anti-PD-L1, and poly(I:C) were administered together (Fig. 1E).

Analysis of TILs showed that neither monotherapy nor combination therapy led to any significant change in the total B and T cells (Supplemental Fig. 2A). However, combination of mGT103 and anti-PD-L1 increased intratumoral cytotoxic $CD8^+$ T cells (Supplemental Fig. 2A). Ag-specific $CD4^+$ T cells were further increased with the combination of mGT103, anti-PD-L1, and poly (I:C) (Supplemental Fig. 2A). Similarly, as shown previously in Fig. 1D, mGT103 induced Ag-specific $CD8^+$ T cells, and the increase was greater when mGT103 was used in combination with either anti-PD-L1 or poly(I:C) or both together (Supplemental Fig. 2A). These data suggest that antitumor activity of mGT103 can be substantially increased when used in combination with anti-PD-L1 therapy, poly(I:C), or both.

The antitumor activity of GT103 depends on both $CD4^+$ and $CD8^+$ T lymphocytes

The impact of mGT103 on intratumoral Tregs, MDSCs, and $CD11c^+$ DCs as well as Ag-specific T cells (Fig. 1) suggested that its antitumor immunity is mediated through T lymphocytes. To establish the roles of T lymphocytes in the mGT103-mediated antitumor effect, we depleted $CD4^+$ and $CD8^+$ T lymphocytes in vivo and treated the tumor-bearing mice with mGT103. Depletion of either $CD4^+$ or $CD8^+$ T cells completely abrogated the antitumor activity of mGT103 (Fig. 2A, 2B). These results demonstrate that the antitumor effect of mGT103 critically depends on both $CD4^+$ and $CD8^+$ T lymphocytes.

GT103 specifically targets tumor-derived CFH

To establish that mGT103 acts by targeting tumor-derived CFH, we compared the growth of s.c. tumors established using WT and CFH-KO CMT167 cells (Fig. 3A). We observed that tumors

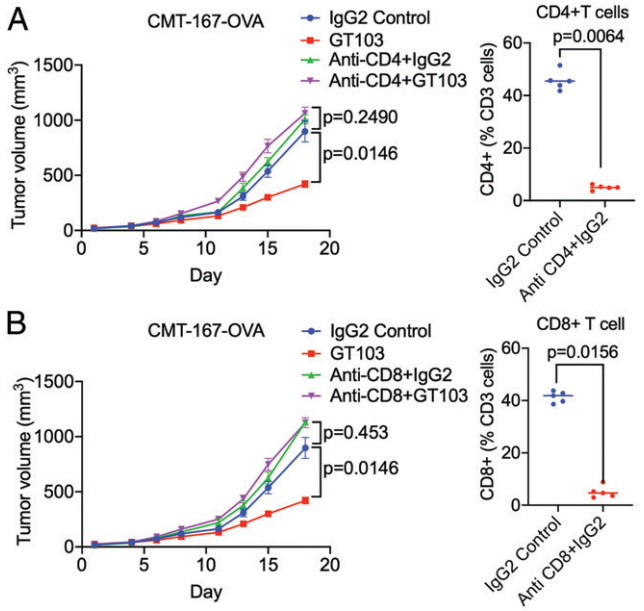

FIGURE 2. Role of T cells in GT103-mediated antitumor activity. Mice were depleted of (**A**) $CD4^+$ or (**B**) $CD8^+$ T cells by injecting respective depleting Abs at 100 μg/mouse i.p. before tumor inoculation. All the mice were inoculated s.c. with 2×10^5 CMT167 cells. When tumors became palpable, mice in each group were dosed three times per week with control IgG2a (200 μg i.p.) or mGT103 (200 μg i.p.) and twice weekly with either anti-CD4 or anti-CD8 depleting Abs. Tumor volume was plotted as mean ± SEM for $n = 5–8$ for each treatment group.

developing from CFH-KO cells did not grow as fast as tumors from WT CMT167 cells, suggesting that tumor-derived CFH plays a major role in tumor growth. In addition, mGT103 did not further inhibit the growth of CFH-KO tumors, confirming GT103 specificity for tumor-derived CFH. Immune cell profiling of these tumors showed that mGT103 did not significantly alter the TME in tumors derived from CFH-KO CMT167 cells (Supplemental Fig. 2B).

An essential role of the complement pathway in GT103-mediated antitumor activity

Although the above data demonstrated T lymphocyte dependency for the antitumor activity of GT103, it is unclear whether this activity is mediated through complement activation or other pathways. To confirm the role of the complement pathway in GT103-mediated antitumor efficacy, we used CVF to deplete C3 in vivo. CVF is a structural and functional analog of the complement component C3 that causes C3 depletion (32). Depletion of C3 abolished antitumor activity of GT103 (Fig. 3B) and maintained the TME in a more immunosuppressive state (Supplemental Fig. 2C). Earlier, we have shown that GT103 causes release of complement activation products C3a and C5a, induces cell death by complement dependent cytotoxicity (CDC) in vitro (5), and increases deposition of C3 split products C3b/iC3b/C3c in tumor tissue (7). Here, we show that blocking C3a and C5a receptors using specific antagonists either alone or in combination completely obliterates the effect of mGT103 (Fig. 3C). In addition, mGT103 treatment of tumors leads to an ~3-fold ($p < 0.001$) increase in expression of the C3 split product C3d on tumor cells (Fig. 3D) as detected by immunoblotting. (Tumors from the same experiment were analyzed here and in reference 7.) C3d binds to its receptor CR2 on B cells and follicular DCs and results in activation of B cells and augmentation of B cell affinity maturation by the follicular DCs displaying these Ags in germinal centers to induce

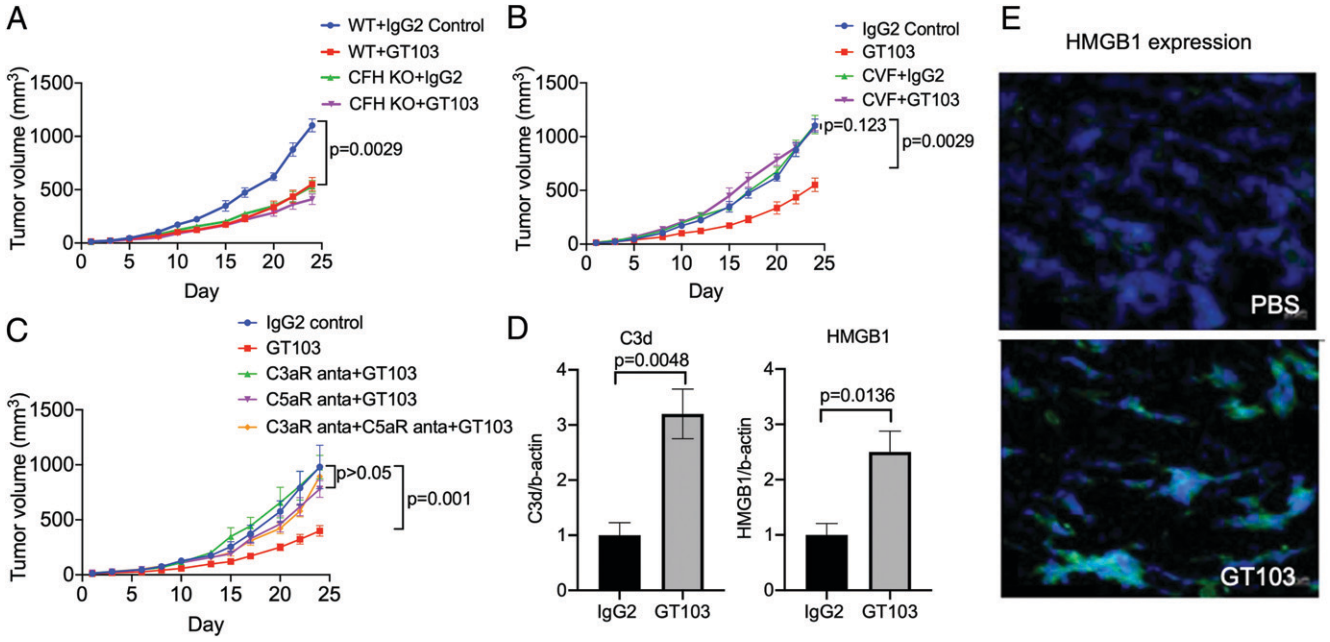

FIGURE 3. Role of complement activation in GT103-mediated antitumor activity. (**A**) Tumors were initiated as described earlier using CMT167 cells and CFH-KO CMT167 cells. After the tumors became palpable, mice were treated either with IgG2a-control Ab or with GT103. CMT167-OVA tumor-bearing mice were treated with (**B**) 10 μg CVF/mouse or (**C**) 1 mg C3aR or C5aR antagonist/kg body weight before being injected with IgG2a or mGT103, and then all treatments were repeated twice weekly. Tumors were measured every other day, and tissue was saved at sacrifice after the end of the treatment period. Tumor volume was plotted as mean ± SEM for $n = 5–8$ for each treatment group. (**D**) Densitometric analysis of Western blots for C3d and HMGB1 normalized to loading control, β-actin, in tumors from GT103-treated mice relative to IgG2a control-treated mice ($n = 4$). (**E**) Immunofluorescence imaging was performed at original magnification ×40 for HMGB1 in tumors of GT103- or control-treated mice. CMT167 tumor sections from GT103-treated or control-treated mice were probed with anti-HMGB1 and Alexa Fluor 488 goat anti-rabbit secondary Ab. with Hoechst 33342 DNA stain.

effector and memory B cell responses (33). Collectively, these findings indicate that the mechanism of mGT103 may be dependent on complement activation that results in the release of C3 split products and anaphylatoxins C3a and C5a that are believed to interact with their receptors on immune cells to stimulate antitumor responses. These results, together with our recent data showing that GT103 causes deposition of C3 fragments on tumor cells and in tumor tissues (7), support the essential role of complement activation in the antitumor efficacy of GT103.

Complement activation and CDC are associated with increased mobilization of damage-associated molecular patterns (DAMPs) (34). We have shown previously that mGT103 increases plasma membrane expression of calreticulin on CMT167 cells both in vitro and in vivo (7). Here, we analyzed the expression of another DAMP, HMGB1, a chromatin-binding protein that is released during late apoptotic or necrotic cell death (35), binds to pattern recognition receptors and TLRs on myeloid cells, and stimulates cross-presentation of tumor Ags. The expression of HMGB1 increased >2-fold ($p < 0.01$) in tumors from mGT103-treated mice as compared with tumors from mice treated with IgG2a control Ab (Fig. 3D). Immunofluorescence imaging also shows increased HMGB1 fluorescence in mGT103-treated CMT167 tumors compared with PBS-treated CMT167 tumors (Fig. 3E).

mGT103 modulates immune signaling pathways in tumor tissues and induces a systemic response

To elucidate the underlying molecular mechanisms of the antitumor effect elicited by mGT103, we performed a transcriptomic analysis of total tumor tissues from mGT103-treated and control mice. Using an initial FDR (q-value) cutoff of <0.05, we identified 4037 differentially expressed genes between mGT103-treated and control tumors that included 2666 upregulated and 1371 downregulated genes in tumors from mGT103-treated compared with control-treated mice. Gene expression was z-score normalized, and the samples and genes were clustered by correlation distance with complete linkage. The heatmap showed markedly different gene expression patterns from the total tumor tissues of control- and mGT103-treated mice (Fig. 4A). To confirm the results of the RNA-seq experiment, we performed quantitative real-time PCR on a subset of the transcripts shown to be elevated following GT103 treatment. Immune activation markers including CTLA-4, IL-2Rα, CCL17, CCL22, integrin-β3, and Slc39a10 were found to be upregulated, validating the RNA-seq data (Fig. 4B).

Gene ontology analysis of significantly enriched processes, components, and functions with an FDR <0.01 showed that the differentially expressed genes were mainly associated with immunologic and metabolic pathways (Fig. 4C). Specifically, the top-ranked differential pathways between mGT103- and control-treated groups included the BCR signaling pathway, regulation of cell–cell adhesion, leukocyte chemotaxis, regulation of IL-1β production, leukocyte migration, regulation of IFN-γ production, regulation of cell activation, and lymphocyte costimulation (Fig. 4C). We further analyzed the differentially expressed genes in the BCR pathway (Supplemental Fig. 3A) and studied the effect of GT103 on B cells in detail using scRNAseq of TILs (7). The heatmap for the top 25 up- and downregulated genes in the B cells is shown in Supplemental Fig. 3B. The hallmark pathway analysis of gene sets with coherent signatures representing biological processes indicated that GT103 treatment led to positive regulation of complement pathway genes, supporting our hypothesis that GT103 exerts its antitumor effect by complement activation. The other positively regulated hallmark pathways by GT103 include G_2-M checkpoint, hypoxia signaling, IL2-STAT5 signaling, IL6-Jak-STAT3 signaling, inflammatory response and TNF-α signaling via NF-κB, all consistent with complement activation and an immune-stimulatory state. On the other

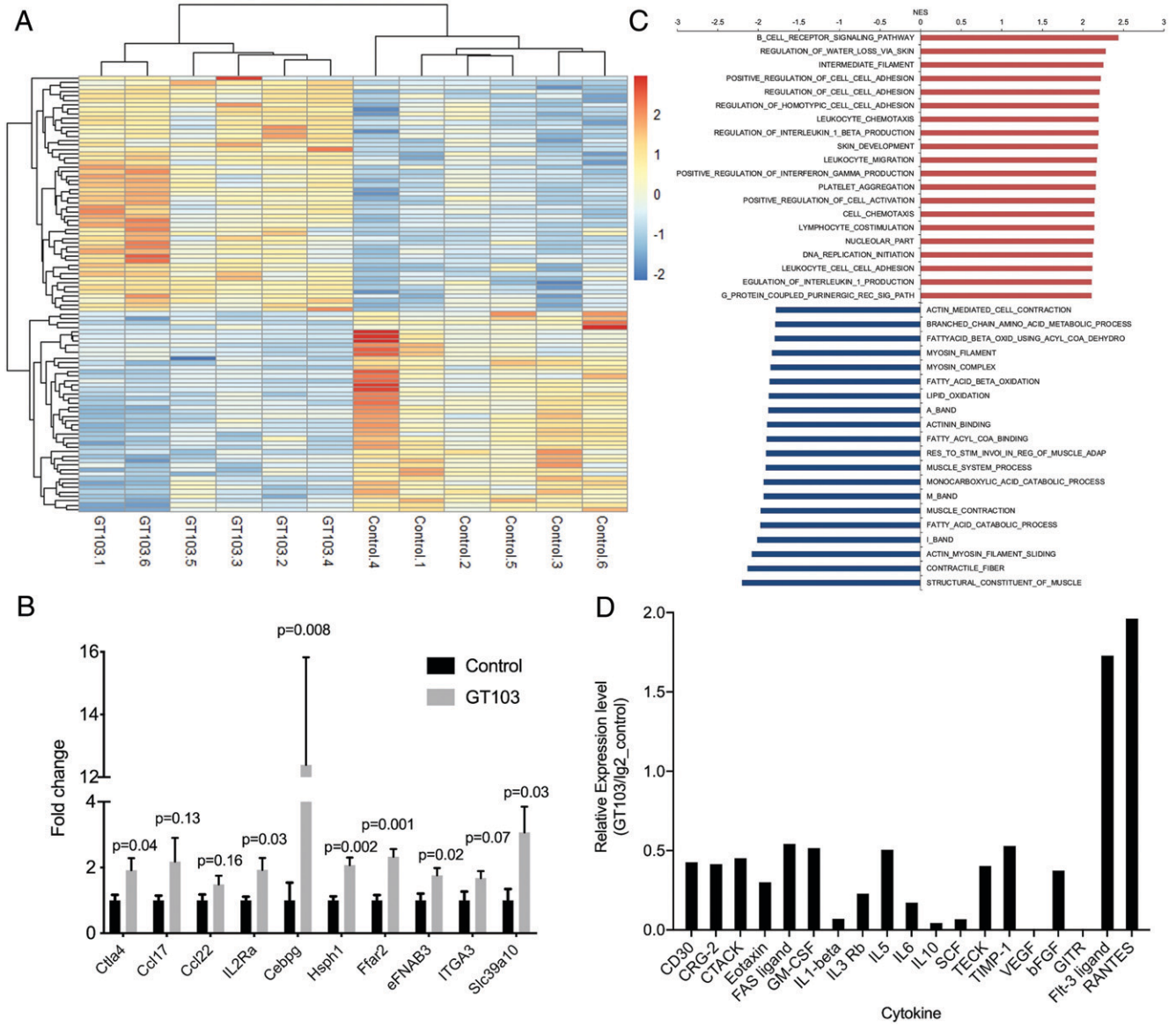

FIGURE 4. RNA-seq analysis of total tumor tissues from GT103-treated mice and systemic effects induced by GT103. (**A**) Heatmap of gene expression in mGT103 and IgG2a control tumors from CMT167 lung cancer–bearing mice. The mRNA levels were expressed as relative fold changes. (**B**) Quantitative PCR detection of gene expression in mGT103-treated and control tumors. The mRNA expression levels were expressed as relative fold changes compared with control. (**C**) List of top 20 cellular pathways that were upregulated or downregulated. Numbers are normalized enrichment score (NES). (**D**) Cytokine levels in the peripheral blood of tumor-bearing mice. Change in level of cytokine was determined using a cytokine array in the pooled sera from tumor-bearing mice treated with PBS and mGT103 at day 0, before treatment, and at day 15, after treatment.

hand, reactive oxygen species (ROS) pathway, IFN-α response, and TGF-β signaling were found to be negatively regulated by GT103.

To investigate whether mGT103 treatment had induced changes in the peripheral blood levels of cytokines and chemokines, we used membrane arrays to measure the levels of 96 different molecules in pooled sera from mGT103-treated and control mice. Several cytokines/chemokines, including Flt3L and Rantes (CCL5), had ~2-fold increased levels in sera of mGT103-treated mice compared with those of control mice (Fig. 1E). Furthermore, serum levels of proinflammatory and protumorigenic cytokines such as IL-1b, IL-5, IL-6, and IL-10 were reduced in mGT103-treated tumor-bearing mice by >50% when compared with control mice. These results indicate that mGT103 treatment in tumor-bearing mice generated an adaptive antitumor immune response. Despite eliciting a systemic immune response, mGT103 does not bind to or cause toxicity in normal tissue as has been established previously (7) and as shown in Supplemental Fig. 3C.

These results demonstrate that GT103 treatment resulted in changes of gene expression in tumor tissues, induced a systemic antitumor response, and provided clues to further probe its antitumor mechanisms.

Molecular pathways in intratumoral lymphocytes upon GT103 treatment

To identify the molecular pathways regulated by mGT103 in intratumoral leukocytes, we performed an unbiased scRNAseq analysis of tumor-infiltrating leukocytes from CMT167 tumors of mGT103- and control-treated mice. Compared with flow cytometric analysis with preselected cellular markers, scRNAseq provided important insights into the infiltrated leukocyte composition of GT103-treated tumors. A total of 16 clusters were identified among the infiltrating leukocytes from both groups (Fig. 5A). Interestingly, cells in the three

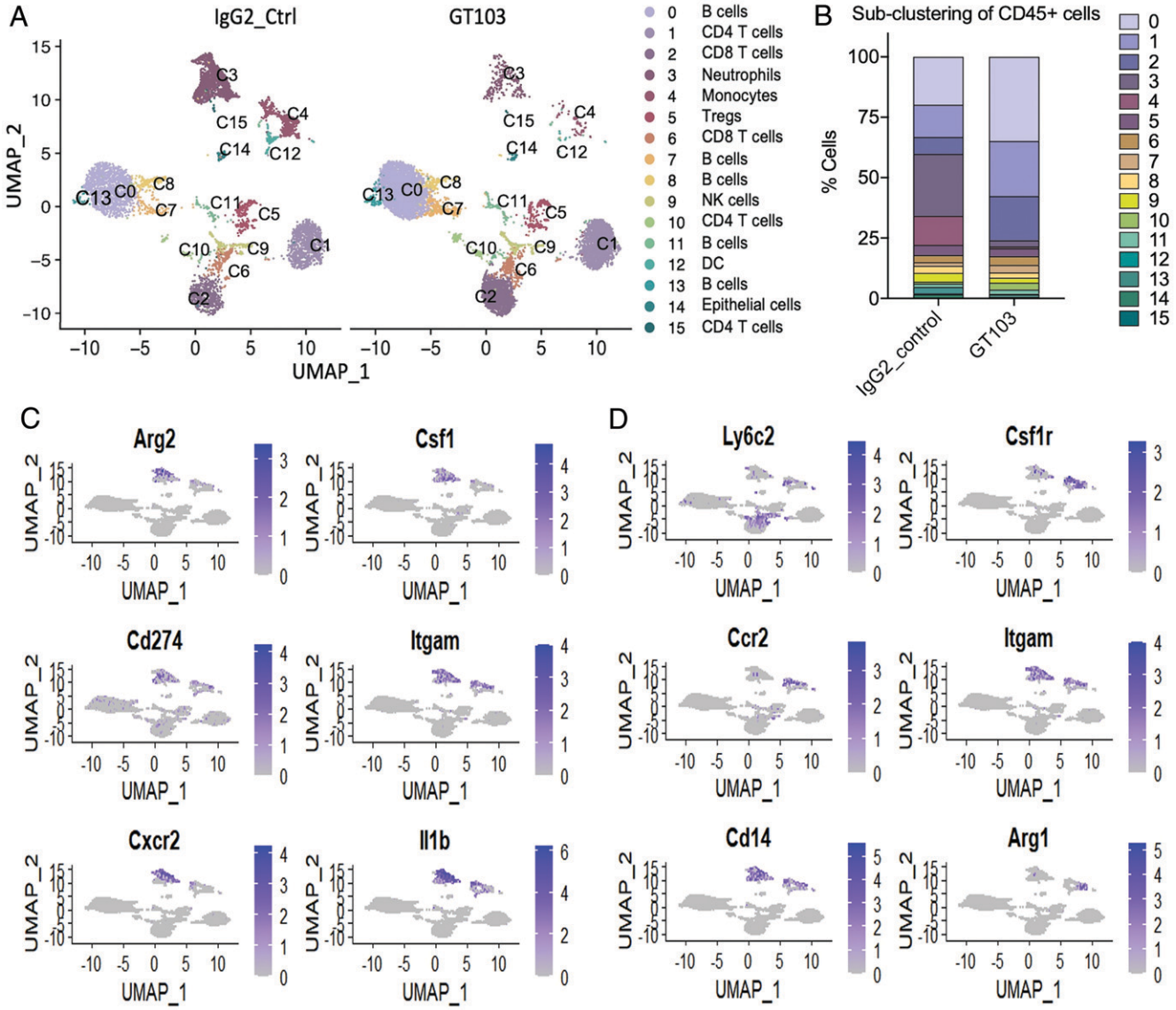

FIGURE 5. scRNAseq expression analysis of TILs from CMT167 tumors treated with GT103 or IgG2a control Ab. After quality control analysis and filtering, 7632 and 6158 cells from mGT103- and control-treated mice, respectively ($n = 3$), were used for analysis. The anchor genes between samples, identified using the FindIntegrationAnchor function, were used as a basis for Seurat to perform integration of the samples. The data were scaled before running principal component analysis. Cluster identification and annotation were performed using a shared nearest neighbor modularity optimization-based clustering algorithm and the FindNeighbors function with 50 principal components, followed by the FindClusters function with the Louvain algorithm using a 0.5 resolution. This allowed assignment of cells to a total of 16 clusters. (**A**) Uniform Manifold Approximation and Projection (UMAP) plots showing distribution of cells per cluster in IgG2_Ctrl versus GT103-treated group. (**B**) The stacked bar chart displaying the distribution of cells by percentage per sample within the main cell clusters in scRNAseq analysis of total TILs. (**C**, **D**) UMAP plots showing the expression of immunosuppressive markers in the (C) neutrophil and (D) monocyte clusters.

clusters that represented a Treg subset of $CD4^+$ T cells, monocytes, and neutrophils were reduced in GT103-treated tumors (Fig. 5B). Analysis of the conserved markers in these three clusters revealed that these cells are immunosuppressive in nature. The $CD4^+$ T cell subcluster expressed FOXP3, characteristic of Tregs. The neutrophil cluster showed strong expression of immunosuppressive genes, including Arg-2, CSF-1, CD-274, CR3/Itgam, Cxcl2, and Il1b, characteristic of the protumor N2 type of tumor-associated neutrophils (TANs) (36, 37) (Fig. 5C). Similarly, the monocytic cluster expressing Ly6c2, csf1r, ccr2, CR3/Itgam, Cd14, and Arg1 corresponded to monocytic MDSC markers (38) (Fig. 5D).

We further subclustered the tumor-infiltrating T cells. Detailed analysis of T cells provided important clues to the role of T cells in mGT103-mediated antitumor activity. A total of 11 T cell clusters were identified (Fig. 6A). Effector $CD8^+$ (cluster 0) T cells were increased, whereas Tregs (cluster 4) were decreased, in mGT103-treated mice (Fig. 6A, 6B). The differentially expressed genes in three important subsets, effector $CD8^+$ (C0), effector $CD4^+$ (C1), and Tregs (C4), exhibited several patterns yielding important functional and mechanistic insights (Fig. 6C, 6E). mRNA expression of positive regulators of T cell function, Cd28, Junb, Cd27, Ccr7, Cd40lg, Cd3g, Gimap1, and Pdcd4, were increased in intratumoral effector $CD8^+$ and $CD4^+$ T cells from mGT103-treated mice. Negative regulators of T cell function, Il1b, Socs3, Tyrobp (Dap12), G0S2, and Irf1, were downregulated in these effector T cells (Fig. 6C, 6D). These changes indicate that mGT103 treatment resulted in overall enhanced effector T cell function. The antiapoptotic gene Bcl-2 was downregulated in both C0 and C1 clusters, indicating that both subsets of T cells are at effector state, as previously reported by our group and others (39, 40). Importantly, mRNA expression

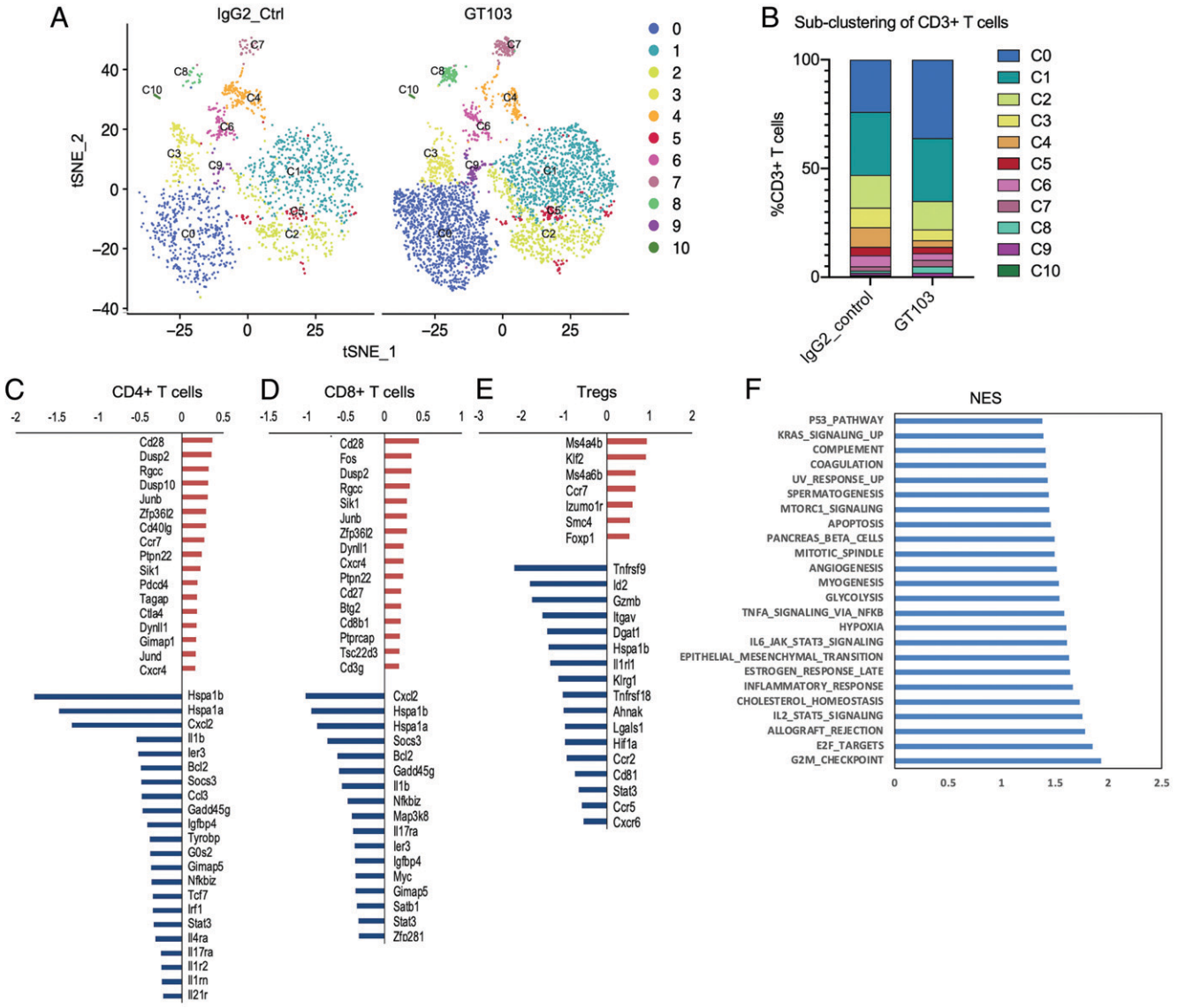

FIGURE 6. Subclustering and gene expression levels in intratumoral T cells. Clusters that were identified as T cells were subsetted for subclustering analysis using the Seurat package. Subclusters in the T subset was identified after running a principal component analysis on the integrated assay of the subset with the graph-based clustering approach implemented in the FindClusters function using 15 principal components and a resolution of 0.5, resulting in 11 T cell subclusters. (**A**) t-Distributed stochastic neighbor embedding (tSNE) plot showing distribution of T cells per cluster in mGT103- and control-treated groups. (**B**) The stacked bar chart displaying the subcluster composition of T cells per sample. Differentially expressed genes in (**C**) $CD4^+$ T cells, (**D**) $CD8^+$ T cells, and (**E**) Treg subclusters between GT103- and control-treated samples. A total of 150–1500 cells were used for differential expression analysis for each cluster ($p < 10^{-6}$ for all listed genes). Scales are $\log_2$. (**F**) Top upregulated pathways in Treg subsets. NES, normalized enrichment score.

of the transcription factor Id2 required for Treg function and its associated Treg-related genes (IL1rl1 [St2], Klrg1, Ccr2, Hif1a) were downregulated (41) (Fig. 6E). In addition, we observed that mGT103 treatment increased activation of pathways, including complement activation–, apoptosis induction–, hypoxia-, and inflammatory response–associated pathways, in the Tregs (Fig. 6F).

Immune landscape of CFH autoantibody-positive patients with lung cancer

The above data from mouse models suggest that the presence of anti-CFH autoantibodies in patients with lung cancer may be associated with a favorable immune landscape in lung cancer tissues. To test this hypothesis, we analyzed the immune landscape of tumor tissues from patients with early-stage lung cancer using IMC, a high-resolution imaging technology. Our previous work identified an association between higher incidence of anti-CFH autoantibodies in patients with early-stage NSCLC (stage I) but not in late-stage patients (3). We selected five stage I anti-CFH Ab–positive patients and five stage I anti-CFH Ab–negative patients with the same adenocarcinoma histology (Supplemental Table S1). We used an IMC Ab panel for human lung cancer analysis containing 22 markers for tumor cells, vascular epithelial cells, and immune cells. The IMC technology allowed us to quantitate immune cell infiltration in the tumor tissue from patients and analyze the spatial relationships of these cells (Fig. 7). Representative images of tumor sections from one each of anti-CFH Ab–positive and anti-CFH Ab–negative patients with NSCLC are shown in Fig. 7A. The figure shows higher representation of immune cell markers and lower abundance of tumor cell markers (smooth muscle actin, vimentin, E-cadherin, and pankeratin) in tumors of anti-CFH Ab–positive patients compared with anti-CFH Ab–negative patients. We further quantified the individual marker intensity of all the samples from the two groups using the

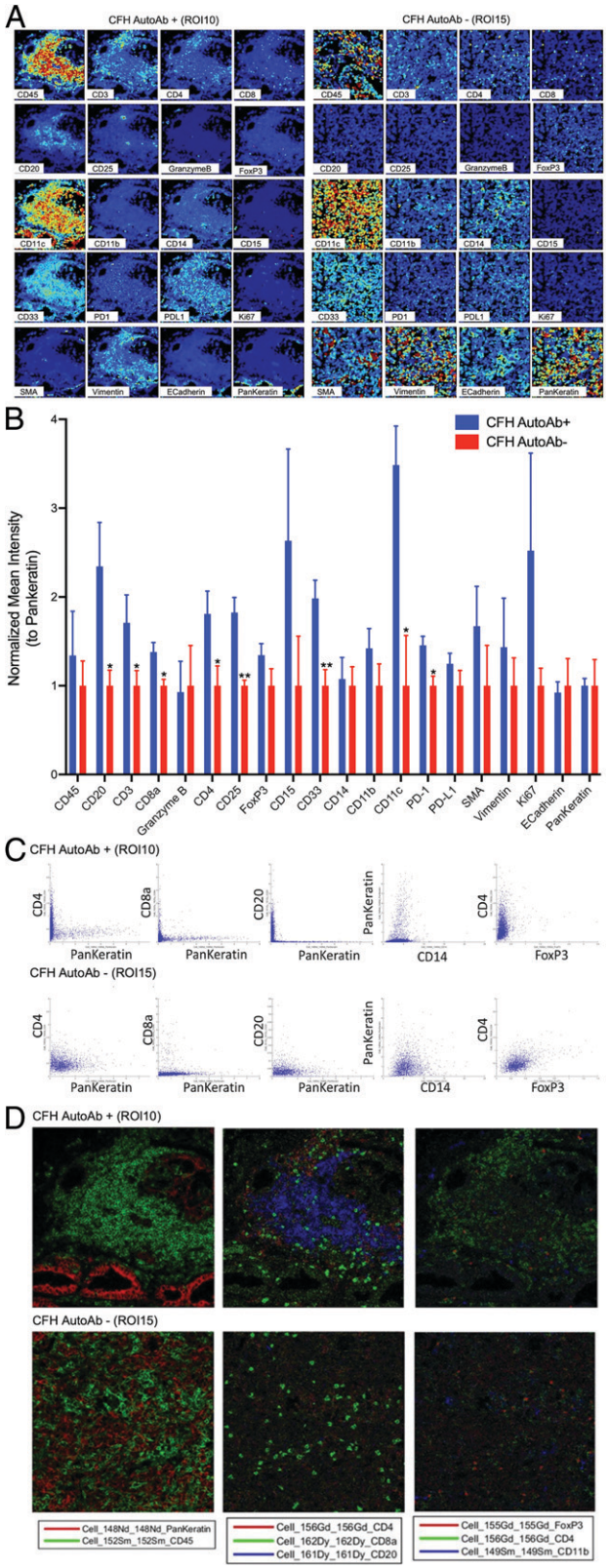

FIGURE 7. IMC analysis of tumor tissue from CFH autoantibody-positive and -negative patients with lung cancer. Tissue sections were stained with a panel of metal-conjugated Abs. Ab staining of tissue sections was quantified through the combination of laser ablation using a modified ArF excimer GeoLas C laser system (Coherent) to ablate tissues in a rastered pattern at 20 Hz and to direct aerosol transportation of the sample to a cytometry by time of flight mass cytometer (Fluidigm). Segmentation was performed using MCDViewer and CellProfiler 4.2.1. MCDViewer was used to classify pixels into three classes (nuclei, membrane, and background) and to generate probability maps. CellProfiler was used to segment probability maps to generate segmentation masks. A combination of channels was used to classify the background and membrane. These masks were combined with the individual .tiff files to extract single-cell information from each individual image, and further analysis was done using HistoCAT_1.73. (**A**) Representative heatmap of the tumor tissue from CFH Ab (+) or (−) patients indicating the intensity of each marker. (**B**) Individual marker intensity was measured by using the histogram function of HistoCAT and then normalized with pankeratin intensity to give normalized mean intensity. Data are plotted as mean ± SEM (n = 5). The p values are denoted as $^{*}p < 0.05$ and $^{**}p < 0.01$. (**C**) Scatterplots indicate the spatial relation of two markers. (*Pan*-keratin is a tumor cell marker.) (**D**) Representative heatmap of the tumor tissue (original magnification ×100) from CFH Ab (+) or (−) patients indicating the distribution of immune cells and cancer cells representing tertiary lymphoid-like structure.

histogram function of histoCAT and normalized it to pankeratin to give normalized mean intensity for all the tissues. We observed a significantly higher percentage of $CD4^+$ helper T cells, $CD8^+$ cytotoxic T cells, $CD20^+$ B cells, $CD11c^+$ DCs, $CD33^+$ cells, and the T cell activation marker $CD25^+$ cells in tumors from anti-CFH Ab–positive patients with NSCLC than in anti-CFH Ab–negative patients (Fig. 7B). One major advantage of the IMC technology is the capability to analyze spatial relationships among various cells. We analyzed the spatial relationships between immune cells and tumor cells in NSCLC patient tumors from the two groups. As shown in Fig. 7C, $CD4^+$, $CD8^+$, and $CD20^+$ effector cells were found to be segregated from $pankeratin^+$ tumor cells in anti-CFH Ab–positive patients with NSCLC, whereas these immune cells were interspersed with tumor cells from the anti-CFH Ab–negative patients with NSCLC. In addition, $FOXP3^+$ cells were more abundant and coexisted with the CD4 marker in the anti-CFH Ab–negative patients with lung cancer, confirming the presence of more Tregs in this group than in the anti-CFH Ab–positive patients with NSCLC. Importantly, $FOXP3^+$ Tregs were in close contact with $Foxp3^-$ $CD4^+$ T cells in the tumors from anti-CFH Ab–negative patients (Fig. 7C). In contrast, the few $FOXP3^+$ Tregs were distant from $FOXP3^-$ $CD4^+$ T cells in the anti-CFH Ab–positive patients (Fig. 7C).

Our observation that the immune cells form clusters in the tumors of anti-CFH Ab–positive patients with NSCLC suggest that tertiary lymphoid-like structures are likely present within these tumors. Indeed, tumors from anti-CFH Ab–positive patients with NSCLC contained $CD45^+$ immune cells forming a core that is surrounded by $pankeratin^+$ tumor cells (Fig. 7D). In contrast, tumors from anti-CFH Ab–negative patients with NSCLC contained $CD45^+$ immune cells that were interspersed with tumor cells (Fig. 7D). Furthermore, $CD4^+/CD8^+$ T and $CD20^+$ B lymphocytes as well as $CD14^+$ myeloid cells aggregated together with $pankeratin^+$ tumor cells in tumors from anti-CFH Ab–positive patients with NSCLC, whereas these immune cells were interspersed with tumor cells in anti-CFH Ab–negative patients with NSCLC (Fig. 7D). Taken together, these IMC analyses revealed a favorable immune landscape in tumors from anti-CFH Ab–positive patients with NSCLC.

Discussion

In this study, we analyzed the cellular and molecular mechanisms of a novel, to our knowledge, mAb derived from an autoantibody discovered in patients with NSCLC with exceptional outcomes to explore how this complement-activating Ab modulates antitumor immunity. The study demonstrated the following. (1) mGT103 has antitumor activities across different tumor types. (2) mGT103 treatment results in a favorable TME, including reduced intratumoral

Tregs, MDSCs, and TANs, and enhanced DCs. (3) mGT103 treatment enhanced Ag-specific tumor-infiltrating T lymphocytes, and its antitumor activity critically depended on $CD4^+$ and $CD8^+$ T lymphocytes. (4) Tumor cell–derived CFH is required for tumor growth in vivo, and mGT103 exerts the antitumor effect by specifically targeting tumor-derived CFH, resulting in activation of the complement pathway. (5) Complement C3 is required for the antitumor activity of mGT103. (6) mGT103 causes accumulation of complement cleavage products C3d and anaphylatoxins C3a and C5a that bind to their receptors on immune cells to stimulate antitumor immunity and mediate CDC and release of DAMPs. (7) mGT103 treatment impacted molecular pathways that are involved in antitumor responses. (8) The immune landscape of tumors from anti-CFH Ab–positive patients with NSCLC is associated with immune activation. (9) The combination of mGT103 with anti-PD-L1 and poly(I:C) further enhances its antitumor efficacy in mice. Previous studies suggested that CFH promotes tumor growth through multiple means, including protection from complement-mediated killing of tumor cells, promotion of $CD14^+$ monocyte differentiation into immune-suppressive (HLA-$DR^{low}$$PD\text{-}L1^{hi}$) macrophages, and differentiation of tolerogenic and anti-inflammatory monocyte-derived DCs (12–19, 22). Our findings suggest that mGT103 blocked CFH and its multiple means of tumor-promoting activities intratumorally.

We show that mGT103 blockade generated a profound change from an immunosuppressive TME to a favorable antitumor setting by decreasing MDSCs and TANs. CFH has been shown to directly promote $CD14^+$ monocyte differentiation into IL-10–producing immunosuppressive macrophages (16). This effect was mediated by binding of the SCR19–20 region of CFH to the monocyte cell surface through unidentified receptor(s), followed by internalization of CFH and intracellular signaling to change the transcriptome into an immunosuppressive signature (16). mGT103, recognizing SCR19 of CFH, may block CFH binding and internalization into monocytes/MDSCs, thereby preventing CFH-mediated intracellular signaling for intratumoral M-MDSC differentiation. Further supporting this, CFH treatment of monocyte-derived DCs generates an anti-inflammatory and tolerogenic state that is also mediated through its SCR19–20 region (22). Our flow cytometric and scRNAseq analyses confirm that mGT103 reduced the influx of immune-suppressive monocytes expressing lLy6c2, csf1r, ccr2, CR3/Itgam, Cd14, and Arg1 markers that correspond to M-MDSC markers (42).

Furthermore, our scRNAseq analysis of intratumoral leukocytes revealed that mGT103 reduced N2-type TANs expressing the immunosuppressive markers Arg2, CSF-1, CD-274, CR3/Itgam, CXCl2, and Il-1b. A possible mechanism of mGT103-induced TAN reduction is through enhanced neutrophil apoptosis. CFH specifically binds to CR3 (CD11b/CD18) on neutrophils through its SCR7 and SCR19–20 domains (43). CFH binding to neutrophils inhibits neutrophil activation, reduces ROS production, and prevents excess inflammation (44, 45). Because ROS is a direct mediator of neutrophil apoptosis (46), mGT103 blocking of CFH binding to CR3 on TANs may result in a loss of CFH inhibition of excess production of ROS, leading to ROS-mediated neutrophil apoptosis in the TME. This hypothesis will be tested in future experiments. The investigation of the impact of mGT103 on intratumoral MDSC and neutrophil fates will be important directions to completely elucidate the roles of this drug in cancer immunotherapy.

Our data demonstrate that mGT103 treatment reduces intratumoral Tregs (itTregs), a major immunosuppressive factor in host antitumor immunity. Several lines of evidence suggest that mGT103 treatment may decrease itTreg survival by suppressing expression of the transcription factor Id2 through C3d engagement of its receptor(s) on itTregs. The CFH-mediated reduction of itTregs may consist of the following cascade. (1) Activation of complement by mGT103 produces an excess level of the complement split product C3d in the TME (47–49). A 3-fold increase in the level of C3d was observed in CMT167 tumors from mGT103-treated mice. (2) C3d engages its receptor CR2 on itTregs and induces itTreg apoptosis and deletion. A recent study showed that tumor-expressed C3d enhances antitumor immunity by depleting itTregs through engagement of its cognate receptor CR2 on itTregs (50). (3) C3d stimulation of CR2 on itTregs downregulates the key transcription factor Id2 and results in impaired function and survival. Both Id2 and Id3 function to maintain peripheral Treg survival (51), whereas Id2 is required for adipose Treg (aTreg) differentiation, survival, and function (41). Loss of Id2 in aTregs resulted in decreased expression of aTreg-associated markers ST2 (IL1rl1), KLRG1, and CCR2, as well as Hif1a (41). ItTregs reside in a hypoxic environment similar to that in adipose tissue. Importantly, our scRNAseq analysis revealed a very similar gene expression pattern between mGT103-treated itTregs and Id2-deficient aTregs, suggesting that mGT103 may trigger a similar signaling cascade to induce itTreg apoptosis.

In addition to the role of T cells, we show that the BCR pathway is activated in mGT103-treated tumors. We have recently demonstrated the importance of B cells in mGT103-mediated antitumor activity (7). That study showed that (1) GT103 activity is dependent on B cells; (2) genes involved in B cell functions (e.g., germinal center formation, MHC class II Ag presentation, Ab production, and survival of mature B cells) are upregulated by mGT103 in intratumoral B cells; and (3) coincubation of tumor cells and B cells in the presence of complement and GT103 leads to B cell activation, presumably due to the release of Ag-conjugated C3d-related complement products that bind to CR2 on B cells (52).

Our analysis of the immune landscapes in tumors from anti-CFH Ab–positive and anti-CFH Ab–negative patients with NSCLC provided further support for the role of mGT103 in creating a favorable TME. The IMC imaging study revealed multiple features of tumors from anti-CFH Ab–positive patients compared with tumors from anti-CFH Ab–negative patients, including (1) higher presentation of effector immune cell populations $CD4^+$ helper T cells, $CD8^+$ cytotoxic T cells, $CD20^+$ B cells, $CD11c^+$ DCs, and the T cell activation marker CD25; (2) less abundant $FOXP3^+$cells; (3) segregation of $CD4^+$, $CD8^+$, and $CD20^+$ effector cells from $pankeratin^+$ tumor cells; and (4) presence of tertiary lymphoid-like structures in anti-CFH Ab–positive patients with NSCLC. Although these findings demonstrate correlation between GT103 and anti-CFH autoantibody, the association may lack causative evidence. A number of other factors may play a role in the generation of a favorable TME and a better outcome apart from the presence of anti-CFH autoantibody in these patients. It is possible that host differences influenced both the formation of autoimmune Abs, including those associated with CFH, and an antitumor microenvironment. As a result, characteristics such as germinal centers may not be related with the presence of anti-CFH autoantibodies but could be driven by an unrelated immune response of the host. Another limitation of the human study is the small sample size and the nonrandom selection of tumors from stage I patients, introducing a potential bias; the autoantibody-positive patients had positive outcomes, whereas autoantibody-negative patients had poor outcomes. The patients selected for their positive outcomes might possess robust antitumor immunity independent of the presence of Abs.

The study also supports our previous findings regarding mGT103-mediated complement activation and its role in tumor growth inhibition. We have previously demonstrated that mGT103 specifically binds to tumor but not normal tissues, causes complement C3 split product deposition on tumor cells, and triggers Ab-dependent cellular phagocytosis (7). Here, we show that tumor-intrinsic CFH is required

for mGT103 antitumor activity and that mGT103 treatment does not bind to (7) or cause toxicity to (5) normal tissues. The role of mGT103 in complement activation was established by loss of mGT103 growth inhibitory activity upon C3 depletion in mice and increased deposition of complement split product C3d on tumor cells. mGT103 also increases expression of the DAMP molecule HMGB1, similar to translocation of another DAMP molecule, calreticulin, to the plasma membrane shown earlier (7). Previously, we reported increased release of anaphylatoxins C3a and C5a and induction of CDC upon mGT103 treatment of tumor cells in vitro (5). The essentiality of these anaphylatoxins for mGT103 activity in vivo was demonstrated by loss of that activity upon blockade of C3a and C5a receptors. Together, these results provide important understanding of the immune-suppressive roles of CFH. The CFH in the tumor microenvironment likely inhibits antitumor immunity by two major modes of action: a direct effect through binding to its receptor CR3 on TAN and MDSCs and an indirect effect through suppressing complement activation. In this model, mGT103 blockade of CFH action in tumors results in reduced MDSC differentiation, increased apoptosis of TANs, and enhanced expansion of effector $CD4^+$ and $CD8^+$ T cells. mGT103, by binding to a tumor-specific epitope in CFH, overcomes CFH-mediated suppression of the alternative complement pathway by causing activation of the classical complement pathway, leading to increased consumption of C3 and to increased production of C3d. C3d binds to CR2 on B cells, causing their activation and expansion, and on Tregs, leading to suppression of Id2 and induction of apoptosis. mGT103 thus creates a highly immune-competent TME to produce antitumor immunity and may serve as an ideal immunotherapeutic drug in both monotherapy and combination therapies.

Last, we found that combination of mGT103 with anti-PD-L1 and the immune adjuvant poly(I:C) exhibits strong antitumor efficacy. Poly(I:C) has no effect on tumor cell growth in vitro, because it functions by engaging TLR3 on APCs to prime an immune-stimulatory effect, and in an in vivo tumor model, it has limited efficacy by itself due to other immunosuppressive factors in the TME. Our data demonstrate the advantage of targeting multiple immunosuppressive effects (i.e., blocking CFH function, targeting PD-L1 immune checkpoint along with enhancing APC functions) using poly(I:C). Our data are consistent with other studies using poly(I:C) to enhance the efficacy of immunotherapeutic agents in several different cancer models. There are 35 Food and Drug Administration–approved combination immunotherapies for various types of cancer (53). The combination immunotherapies for NSCLC primarily consist of anti-PD-1/PD-L1 mAbs plus chemotherapies (53). The data from our current phase Ib clinical trial (NCT04314089) in patients with advanced stage refractory NSCLC has established an exceptional safety profile for GT103. The drug was well tolerated and has shown no adverse impact on renal function or any significant adverse events (54). However, GT103 monotherapy may not be sufficient to control late-stage cancer. The enhanced antitumor efficacy by combined use of mGT103 with anti-PD-L1 plus poly(I:C) provides an important clue for the next phase of clinical trials. A phase II trial combining GT103 and Keytruda for patients with advanced, refractory NSCLC is now open for enrollment (NCT05617313). The present study serves to emphasize the importance of not only targeting tumor epitopes but also activating complement in Ab-based antitumor therapy to promote an immune program with the potential for a durable, meaningful clinical response. Further studies will be useful to better understand the effect of an anti-CFH Ab on antitumor immunity and the optimal population that will respond to therapy.

Disclosures

E.F.P. is a founder, board member, and the chief executive officer of Grid Therapeutics, LLC. M.J.C. and E.B.G. are founders of Grid Therapeutics, LLC. R.S., R.T.B., J.G., and Y.-W.H. declare no conflicts of interest.

References

1. Carmi, Y., M. H. Spitzer, I. L. Linde, B. M. Burt, T. R. Prestwood, N. Perlman, M. G. Davidson, J. A. Kenkel, E. Segal, G. V. Pusapati, et al. 2015. Allogeneic IgG combined with dendritic cell stimuli induce antitumour T-cell immunity. *Nature* 521: 99–104.
2. Ricklin, D., G. Hajishengallis, K. Yang, and J. D. Lambris. 2010. Complement: a key system for immune surveillance and homeostasis. *Nat. Immunol.* 11: 785–797.
3. Amornsiripanitch, N., S. Hong, M. J. Campa, M. M. Frank, E. B. Gottlin, and E. F. Patz, Jr. 2010. Complement factor H autoantibodies are associated with early stage NSCLC. *Clin. Cancer Res.* 16: 3226–3231.
4. Campa, M. J., E. B. Gottlin, R. T. Bushey, and E. F. Patz, Jr. 2015. Complement factor H antibodies from lung cancer patients induce complement-dependent lysis of tumor cells, suggesting a novel immunotherapeutic strategy. *Cancer Immunol. Res.* 3: 1325–1332.
5. Bushey, R. T., M. A. Moody, N. L. Nicely, B. F. Haynes, S. M. Alam, S. T. Keir, R. C. Bentley, K. Roy Choudhury, E. B. Gottlin, M. J. Campa, et al. 2016. A therapeutic antibody for cancer, derived from single human B cells. *Cell Rep.* 15: 1505–1513.
6. Bushey, R. T., E. B. Gottlin, M. J. Campa, and E. F. Patz, Jr. 2021. Complement factor H protects tumor cell-derived exosomes from complement-dependent lysis and phagocytosis. *PLoS One* 16: e0252577.
7. Bushey, R. T., R. Saxena, M. J. Campa, E. B. Gottlin, Y. He, and E. F. Patz. 2023. Antitumor immune mechanisms of the anti-complement factor H antibody GT103. *Mol. Cancer Ther.* 22: 778–789.
8. Blanc, C., L. T. Roumenina, Y. Ashraf, S. Hyvarinen, S. K. Sethi, B. Ranchin, P. Niaudet, C. Loirat, A. Gulati, A. Bagga, et al. 2012. Overall neutralization of complement factor H by autoantibodies in the acute phase of the autoimmune form of atypical hemolytic uremic syndrome. *J. Immunol.* 189: 3528–3537.
9. Reis, E. S., D. C. Mastellos, D. Ricklin, A. Mantovani, and J. D. Lambris. 2018. Complement in cancer: untangling an intricate relationship. *Nat. Rev. Immunol.* 18: 5–18.
10. Roumenina, L. T., M. V. Daugan, F. Petitprez, C. Sautes-Fridman, and W. H. Fridman. 2019. Context-dependent roles of complement in cancer. *Nat. Rev. Cancer* 19: 698–715.
11. Saxena, R., E. B. Gottlin, M. J. Campa, R. T. Bushey, J. Guo, E. F. Patz, Jr., and Y.-W. He. 2024. Complement factor H: a novel innate immune checkpoint in cancer immunotherapy. *Front. Cell Dev. Biol.* 12: 1302490.
12. Ajona, D., Z. Castano, M. Garayoa, E. Zudaire, M. J. Pajares, A. Martinez, F. Cuttitta, L. M. Montuenga, and R. Pio. 2004. Expression of complement factor H by lung cancer cells: effects on the activation of the alternative pathway of complement. *Cancer Res.* 64: 6310–6318.
13. Ajona, D., Y. F. Hsu, L. Corrales, L. M. Montuenga, and R. Pio. 2007. Down-regulation of human complement factor H sensitizes non-small cell lung cancer cells to complement attack and reduces in vivo tumor growth. *J. Immunol.* 178: 5991–5998.
14. Varsano, S., L. Rashkovsky, H. Shapiro, D. Ophir, and T. Mark-Bentankur. 1998. Human lung cancer cell lines express cell membrane complement inhibitory proteins and are extremely resistant to complement-mediated lysis; a comparison with normal human respiratory epithelium in vitro, and an insight into mechanism(s) of resistance. *Clin. Exp. Immunol.* 113: 173–182.
15. Wilczek, E., R. Rzepko, D. Nowis, M. Legat, J. Golab, M. Glab, A. Gorlewicz, F. Konopacki, M. Mazurkiewicz, D. Sladowski, et al. 2008. The possible role of factor H in colon cancer resistance to complement attack. *Int. J. Cancer* 122: 2030–2037.
16. Smolag, K. I., C. M. Mueni, K. Leandersson, K. Jirstrom, C. Hagerling, M. Morgelin, P. N. Barlow, M. Martin, and A. M. Blom. 2020. Complement inhibitor factor H expressed by breast cancer cells differentiates $CD14^+$ human monocytes into immunosuppressive macrophages. *Oncoimmunology* 9: 1731135.
17. Junnikkala, S., T. S. Jokiranta, M. A. Friese, H. Jarva, P. F. Zipfel, and S. Meri. 2000. Exceptional resistance of human H2 glioblastoma cells to complement-mediated killing by expression and utilization of factor H and factor H-like protein 1. *J. Immunol.* 164: 6075–6081.
18. Junnikkala, S., J. Hakulinen, H. Jarva, T. Manuelian, L. Bjorge, R. Butzow, P. F. Zipfel, and S. Meri. 2002. Secretion of soluble complement inhibitors factor H and factor H-like protein (FHL-1) by ovarian tumour cells. *Br. J. Cancer* 87: 1119–1127.
19. Fedarko, N. S., B. Fohr, P. G. Robey, M. F. Young, and L. W. Fisher. 2000. Factor H binding to bone sialoprotein and osteopontin enables tumor cell evasion of complement-mediated attack. *J. Biol. Chem.* 275: 16666–16672.
20. Cui, T., Y. Chen, T. Knosel, L. Yang, K. Zoller, K. Galler, A. Berndt, M. Mihlan, P. F. Zipfel, and I. Petersen. 2011. Human complement factor H is a novel diagnostic marker for lung adenocarcinoma. *Int. J. Oncol.* 39: 161–168.
21. Daugan, M. V., M. Revel, R. Thouenon, M. A. Dragon-Durey, T. Robe-Rybkine, C. Torset, N. S. Merle, R. Noe, V. Verkarre, S. M. Oudard, et al. 2021. Intracellular factor H drives tumor progression independently of the complement cascade. *Cancer Immunol. Res.* 9: 909–925.
22. Olivar, R., A. Luque, S. Cardenas-Brito, M. Naranjo-Gomez, A. M. Blom, F. E. Borras, S. Rodriguez de Cordoba, P. F. Zipfel, and J. M. Aran. 2016. The

complement inhibitor factor H generates an anti-inflammatory and tolerogenic state in monocyte-derived dendritic cells. *J. Immunol.* 196: 4274–4290.
23. Mao, X., L. Zhou, S. K. Tey, A. P. Y. Ma, C. L. S. Yeung, T. H. Ng, S. W. K. Wong, B. H. M. Liu, Y. M. E. Fung, E. F. Patz, Jr., et al. 2020. Tumour extracellular vesicle-derived complement factor H promotes tumorigenesis and metastasis by inhibiting complement-dependent cytotoxicity of tumour cells. *J. Extracell. Vesicles* 10: e12031.
24. Shu, C., H. Zha, H. Long, X. Wang, F. Yang, J. Gao, C. Hu, L. Zhou, B. Guo, and B. Zhu. 2020. C3a-C3aR signaling promotes breast cancer lung metastasis via modulating carcinoma associated fibroblasts. *J. Exp. Clin. Cancer Res.* 39: 11.
25. Jiang, K., S. Lu, D. Li, M. Liu, H. Jin, B. Lei, S. Wang, K. Long, S. He, and F. Zhong. 2023. Blockade of C5aR1 alleviates liver inflammation and fibrosis in a mouse model of NASH by regulating TLR4 signaling and macrophage polarization. *J. Gastroenterol.* 58: 894–907.
26. McCarthy, D. J., K. R. Campbell, A. T. Lun, and Q. F. Wills. 2017. Scater: preprocessing, quality control, normalization and visualization of single-cell RNA-seq data in R. *Bioinformatics* 33: 1179–1186.
27. Stuart, T., A. Butler, P. Hoffman, C. Hafemeister, E. Papalexi, W. M. Mauck, 3rd, Y. Hao, M. Stoeckius, P. Smibert, and R. Satija. 2019. Comprehensive integration of single-cell data. *Cell* 177: 1888–1902.e21.
28. Tseng, G. C., D. Ghosh, and E. Feingold. 2012. Comprehensive literature review and statistical considerations for microarray meta-analysis. *Nucleic Acids Res.* 40: 3785–3799.
29. Aran, D., A. P. Looney, L. Liu, E. Wu, V. Fong, A. Hsu, S. Chak, R. P. Naikawadi, P. J. Wolters, A. R. Abate, et al. 2019. Reference-based analysis of lung single-cell sequencing reveals a transitional profibrotic macrophage. *Nat. Immunol.* 20: 163–172.
30. Heng, T. S., M. W. Painter, and, and G. P. Immunological, C. 2008. The Immunological Genome Project: networks of gene expression in immune cells. *Nat. Immunol.* 9: 1091–1094.
31. Schapiro, D., H. W. Jackson, S. Raghuraman, J. R. Fischer, V. R. T. Zanotelli, D. Schulz, C. Giesen, R. Catena, Z. Varga, and B. Bodenmiller. 2017. histoCAT: analysis of cell phenotypes and interactions in multiplex image cytometry data. *Nat. Methods* 14: 873–876.
32. Wang, S. Y., S. Veeramani, E. Racila, J. Cagley, D. C. Fritzinger, C. W. Vogel, W. St John, and G. J. Weiner. 2009. Depletion of the C3 component of complement enhances the ability of rituximab-coated target cells to activate human NK cells and improves the efficacy of monoclonal antibody therapy in an in vivo model. *Blood* 114: 5322–5330.
33. Merle, N. S., R. Noe, L. Halbwachs-Mecarelli, V. Fremeaux-Bacchi, and L. T. Roumenina. 2015. Complement system part II: role in immunity. *Front. Immunol.* 6: 257.
34. Kataoka, H., H. Kono, Z. Patel, Y. Kimura, and K. L. Rock. 2014. Evaluation of the contribution of multiple DAMPs and DAMP receptors in cell death-induced sterile inflammatory responses. *PLoS One* 9: e104741.
35. Fabian, K. P., B. Wolfson, and J. W. Hodge. 2021. From immunogenic cell death to immunogenic modulation: select chemotherapy regimens induce a spectrum of immune-enhancing activities in the tumor microenvironment. *Front. Oncol.* 11: 728018.
36. Masucci, M. T., M. Minopoli, and M. V. Carriero. 2019. Tumor associated neutrophils. Their role in tumorigenesis, metastasis, prognosis and therapy. *Front. Oncol.* 9: 1146.
37. Shaul, M. E., L. Levy, J. Sun, I. Mishalian, S. Singhal, V. Kapoor, W. Horng, G. Fridlender, S. M. Albelda, and Z. G. Fridlender. 2016. Tumor-associated neutrophils display a distinct N1 profile following TGFbeta modulation: a transcriptomics analysis of pro- vs. antitumor TANs. *Oncoimmunology* 5: e1232221.
38. Hegde, S., A. M. Leader, and M. Merad. 2021. MDSC: markers, development, states, and unaddressed complexity. *Immunity* 54: 875–884.
39. Dunkle, A., I. Dzhagalov, C. Gordy, and Y. W. He. 2013. Transfer of $CD8^+$ T cell memory using Bcl-2 as a marker. *J. Immunol.* 190: 940–947.
40. Grayson, J. M., A. J. Zajac, J. D. Altman, and R. Ahmed. 2000. Cutting edge: increased expression of Bcl-2 in antigen-specific memory $CD8^+$ T cells. *J. Immunol.* 164: 3950–3954.
41. Frias, A. B. Jr., E. J. Hyzny, H. M. Buechel, L. Y. Beppu, B. Xie, M. J. Jurczak, and L. M. D'Cruz. 2019. The transcriptional regulator Id2 is critical for adipose-resident regulatory T cell differentiation, survival, and function. *J. Immunol.* 203: 658–664.
42. Alshetaiwi, H., N. Pervolarakis, L. L. McIntyre, D. Ma, Q. Nguyen, J. A. Rath, K. Nee, G. Hernandez, K. Evans, L. Torosian, et al. 2020. Defining the emergence of myeloid-derived suppressor cells in breast cancer using single-cell transcriptomics. *Sci. Immunol.* 5: eaay6017
43. Losse, J., P. F. Zipfel, and M. Jozsi. 2010. Factor H and factor H-related protein 1 bind to human neutrophils via complement receptor 3, mediate attachment to *Candida albicans*, and enhance neutrophil antimicrobial activity. *J. Immunol.* 184: 912–921.
44. Schneider, A. E., N. Sandor, E. Karpati, and M. Jozsi. 2016. Complement factor H modulates the activation of human neutrophil granulocytes and the generation of neutrophil extracellular traps. *Mol. Immunol.* 72: 37–48.
45. Chen, S. F., F. M. Wang, Z. Y. Li, F. Yu, M. Chen, and M. H. Zhao. 2018. Complement factor H inhibits anti-neutrophil cytoplasmic autoantibody-induced neutrophil activation by interacting with neutrophils. *Front. Immunol.* 9: 559.
46. Kasahara, Y., K. Iwai, A. Yachie, K. Ohta, A. Konno, H. Seki, T. Miyawaki, and N. Taniguchi. 1997. Involvement of reactive oxygen intermediates in spontaneous and CD95 (Fas/APO-1)-mediated apoptosis of neutrophils. *Blood* 89: 1748–1753.
47. Licht, C., A. Weyersberg, S. Heinen, L. Stapenhorst, J. Devenge, B. Beck, R. Waldherr, M. Kirschfink, P. F. Zipfel, and B. Hoppe. 2005. Successful plasma therapy for atypical hemolytic uremic syndrome caused by factor H deficiency owing to a novel mutation in the complement cofactor protein domain 15. *Am. J. Kidney Dis.* 45: 415–421.
48. Wehling, C., O. Amon, M. Bommer, B. Hoppe, K. Kentouche, G. Schalk, R. Weimer, M. Wiesener, B. Hohenstein, B. Tonshoff, et al. 2017. Monitoring of complement activation biomarkers and eculizumab in complement-mediated renal disorders. *Clin. Exp. Immunol.* 187: 304–315.
49. Westra, D., E. B. Volokhina, R. G. van der Molen, T. J. van der Velden, A. Jeronimus-Klaasen, J. Goertz, V. Gracchi, E. M. Dorresteijn, A. H. Bouts, M. G. Keijzer-Veen, et al. 2017. Serological and genetic complement alterations in infection-induced and complement-mediated hemolytic uremic syndrome. *Pediatr. Nephrol.* 32: 297–309.
50. Platt, J. L., I. Silva, S. J. Balin, A. R. Lefferts, E. Farkash, T. M. Ross, M. C. Carroll, and M. Cascalho. 2017. C3d regulates immune checkpoint blockade and enhances antitumor immunity. *JCI Insight* 2: e90201.
51. Miyazaki, M., K. Miyazaki, S. Chen, M. Itoi, M. Miller, L. F. Lu, N. Varki, A. N. Chang, D. H. Broide, and C. Murre. 2014. Id2 and Id3 maintain the regulatory T cell pool to suppress inflammatory disease. *Nat. Immunol.* 15: 767–776.
52. Carroll, M. C., and D. E. Isenman. 2012. Regulation of humoral immunity by complement. *Immunity* 37: 199–207.
53. Lu, L., M. Zhan, X. Y. Li, H. Zhang, D. J. Dauphars, J. Jiang, H. Yin, S. Y. Li, S. Luo, Y. Li, and Y. W. He. 2022. Clinically approved combination immunotherapy: current status, limitations, and future perspective. *Curr. Res. Immunol.* 3: 118–127.
54. Clarke, J. M., T. E. Stinchcombe, J. Crawford, H. M. Mamdani, L. Gu, N. Ready, A. Nixon, S. Baleviic, M. J. Campa, E. B. Gottlin, et al. 2022. Interim results from a phase IB, first-in-human study of a novel complement factor H inhibitor (GT103) in patients with refractory non-small cell lung cancer (NSCLC) [abstract]. *J. Immunother. Cancer* 10(Suppl 2): 699.